

COMPUTATION OF TURBULENT HEAT TRANSFER IN A SQUARE DUCT WITH ONE ROUGHENED WALL BY USING ALGEBRAIC HEAT FLUX MODELS

Hitoshi SUGIYAMA

Graduate School of Engineering, Utsunomiya University
 7-1-2 Yoto, Utsunomiya, 321-8585 Japan
 sugiyama@cc.utsunomiya-u.ac.jp

Masahiro TOSEN

Graduate School of Engineering,
 Utsunomiya University
 7-1-2 Yoto, Utsunomiya, 321-8585 Japan

Fred B. GESSNER

Department of Mechanical Engineering,
 University of Washington
 Box 352600, Seattle, WA 98195-2600, USA
 gessnerf@u.washington.edu

Keywords: Square duct flow, Rib-roughened wall, Secondary flow, Turbulent heat flux components

ABSTRACT

Calculations have been performed for fully developed turbulent flow and heat transfer in a square duct with one roughened wall. Figure A-1 shows the coordinate system and the schematic diagram of a square duct with one roughened wall. This paper focuses on the application of three algebraic models of the turbulent heat flux transport equation in order to predict turbulent heat flux component behavior. The convection and diffusion terms in this transport equation are modeled in a manner similar to Rodi's approximation for corresponding terms in the Reynolds stress transport equations. The pressure-temperature gradient term is simulated by means of three models: one a composite based on the "slow" and "rapid" interaction models proposed by Lumley and Launder (LL), respectively, and another, the model proposed by Shih and Lumley (SL), and the other, the model proposed by Craft and Launder (CL). These three models lead to predicted mean temperature distributions in the duct cross plane that are in relatively good agreement with experimentally measured distributions as shown in Figure A-2. In Figure A-2, three calculated results are displayed in left hand side of each figure. It has been pointed out as a characteristic feature that the contour lines are distorted by the secondary flow of the second kind near the upper smooth wall. Adding to this,

calculated turbulent heat flux component distributions in the cross plane show that the three models predict experimentally observed features in the flow. Considering that the pressure-temperature gradient term of CL model is composed of many terms compared with the other two models, calculated results have suggested that the turbulent heat flux distributions in a square duct with one roughened wall could be predicted well by adopting simple model such as LL and SL models.

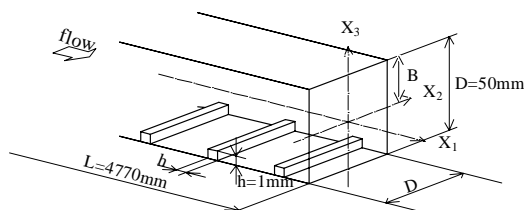


Figure A-1 Coordinate system and schematic diagram of a square duct with roughened wall

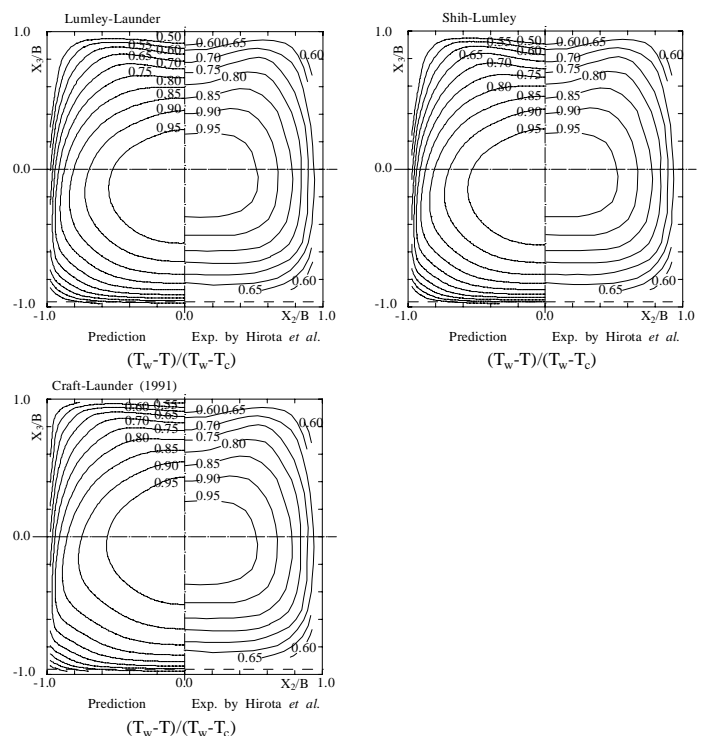


Figure A-2 Calculated results of mean temperature distributions in the duct cross plane

INTRODUCTION

In some square duct heat exchanger applications, one or more walls of the duct are roughened in order to enhance heat transfer between the flowing fluid and the duct surroundings. The efficiency of the process depends greatly on the nature of the roughened wall. For example, with periodically spaced, rib-type roughness elements installed normal to the primary flow direction, heat transfer across the wall is enhanced with minimal increase in pressure drop, provided that the height of the roughness elements is small compared to the duct height. Research on turbulent flow in square ducts with one or more rib-roughened walls can be classified into two types of basic studies: those concerned with local flow and heat transfer in the vicinity of a rib-roughened wall and those concerned with global flow and heat transfer behavior across the entire duct cross section. The present study lies within the latter category, and focuses on the nature of temperature and turbulent heat flux distributions in the duct cross plane, as influenced by one roughened wall for fully-developed flow conditions. In reference to previous research in this area, Humphrey and Whitelaw [1], Fujita et al. [2], [3], [4], and Yokosawa et al. [5] have measured mean flow and turbulence properties in a square duct having one or more rib-roughened walls. The results of Fujita et al. [3], for example, show that the overall flow pattern in a square duct with one rib-roughened wall does not depend strongly on whether measurements are made in the duct cross section directly over a rib or midway between adjacent ribs, provided the rib height (h) compared to the duct height (H) is small ($h/H=0.02$ for the operating conditions of that study). This conclusion provides justification for treating a rib-roughened wall as one of uniform roughness for cross-planar flow predictions when the flow is fully developed, as is done in the present study.

In reference to numerical analyses of square duct flow with one roughened wall, the predictions of Sugiyama et al. [6] are in relatively good agreement with experimental distributions measured by Fujita et al. [3], which include primary flow velocity, secondary flow velocity, turbulence kinetic energy and Reynolds stress anisotropy distributions in the cross plane. Their turbulence model consists of transport equations for k and ϵ in conjunction with an algebraic stress model based on the pressure-strain model proposed Gessner and Eppich [7] and Rodi's [8] approximation for the convection and diffusion terms in the Reynolds stress transport equations. In a more recent study, Naimi and Gessner [9] have shown that even better agreement with Fujita et al.'s data is possible if the Reynolds stress transport equation model developed by Naimi and Gessner [10] is applied to a square duct flow with one roughened wall.

Heat transfer measurements and predictions in square ducts with one or more roughened walls are fairly scarce. For the case of fully developed flow and heat transfer in a square duct with either two opposite, or all four, rib-roughened walls, Fujita et al.[2] predicted

temperature contours in the duct cross plane and local wall heat flux distributions, but no comparisons with experimental data were made. In a subsequent study, Sugiyama et al.[11] compared their predictions with experimental results presented by Hirota et al. [12], which include mean temperature distributions in the duct cross plane, as well as local Nusselt number distributions along the smooth walls of the duct opposite and adjacent to a rib-roughened wall. Recently, Hirota et al. [13], present cross planar distributions of the three turbulent heat flux components ($-u_i T', i = 1, 2, 3$), as measured in a square duct with one rib-roughened wall. Measurements such as these provide valuable data from the standpoint of assessing proposed models of the turbulent heat flux transport equation.

The precise modeling of turbulent heat flux behavior is especially important if the temperature field is to be predicted accurately in duct flows dominated by secondary flow effects (e.g., square duct flow with or without roughened walls). Furthermore, accurate modeling of the pressure-temperature gradient term in the turbulent heat flux transport equation is just as important as modeling the pressure-strain term in the Reynolds stress transport equations accurately for good predictions of the both the mean velocity and mean temperature fields. From this point of view, Sugiyama et al. [14] have calculated the turbulent heat flux distributions which have measured by Hirota et al.[12] in order to show the difference between Lumley and Launder model (LL), and Jones and Musonge model (JM). They have presented that the LL model predicts the turbulent heat flux distributions better than JM model. As for the turbulent heat flux model, the other several models have been proposed up to now, for example, one is Shih and Lumuly model (SL), and the other is the Craft and Launder model (CL). The purpose of the present study is to investigate the predictive capabilities of three algebraic versions of the turbulent heat flux transport equation based on three different models for the pressure-temperature gradient term which appears in this equation. In this study, the LL, SL and CL models are adopted to investigate the capabilities of turbulent heat flux. The flow situation considered is that of fully developed flow and heat transfer in a square duct with one rib-roughened wall.

NOMENCLATURE

A	thermal diffusivity
B	duct half width (Fig. 1)
C_μ	coefficient
D	duct width (Fig. 1)
D_h	hydraulic diameter
h	rib height
H	duct height ($H=D$ for a square duct)
k	turbulence kinetic energy
L	characteristic length
p	fluctuating static pressure
P	mean static pressure
P_k	turbulence kinetic energy production rate

Re Reynolds number ($=U_b D_h / \nu$)
 t time
 T_c axial centerline temperature
 T_w wall temperature
 T' temperature fluctuation
 u_i i 'th fluctuating velocity component; $i=1,2,3$
 $\overline{u_i T'}$ i 'th turbulent heat flux correlation; $i=1,2,3$
 $\overline{u_i u_j}$ Reynolds stress tensor; $i=1,2,3$
 U_b bulk velocity
 U_c axial centerline velocity
 U_i i 'th mean velocity component; $i=1,2,3$
 U friction velocity ($=\sqrt{\tau_w / \rho}$)
 X_i i 'th Cartesian coordinate; $i=1,2,3$
 X_w wall coordinate

Greek

ϵ Isotropic dissipation rate
 ϵ_{ij} dissipation rate tensor
 K Von Karman's constant ($=0.42$)
 ν Kinematic viscosity
 ρ fluid density
 τ_w wall shear stress

Special

$\overline{(\quad)}$ Time averaged correlation

PHYSICAL FLOW SITUATION

The duct configuration and coordinate axes are shown in Fig. 1. The operating conditions correspond to those employed by Hirota et al. [12],[15]. In brief, their experimental configuration consisted of a square duct, 50mm \times 50mm in cross section, with an overall length of 4770 mm ($=94.5D$) and nominally uniform flow at the duct inlet ($X_1 = 0$). The unheated portion of the duct consisted of a 3020 mm long section, which yielded fully developed turbulent flow at the entrance to the heated section (at $X_1 / D = 60.4$). This section, which consisted of 10mm thick aluminum walls and extended from $X_1 / D = 60.4$ to $X_1 / D = 94.5$, was surrounded by a constant temperature steam bath at 373 K (100C). The

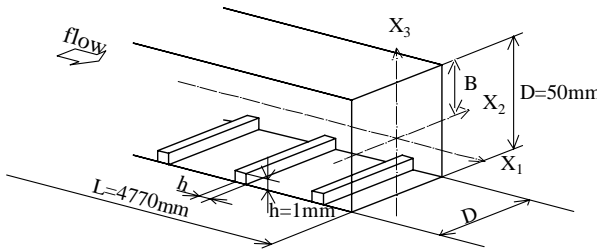


Figure 1 Coordinate system and schematic diagram of a square duct with one roughened wall

rib-roughened wall shown in Fig. 1 was generated by machining square ribs, 1mm \times 1mm in cross section, directly on one wall with a periodic spacing of 10mm between adjacent ribs over the length of the duct. Measurements were made in the duct cross section near the end of the duct midway between adjacent ribs (at $X_1 / D = 93.4$) where both the mean temperature and mean velocity fields were fully developed. The operating Reynolds number was 6.5×10^4 based on properties evaluated at the entrance of the heated section.

MATHEMATICAL MODEL

Flow field model

Inasmuch as the above flow situation corresponds to incompressible flow with essentially constant thermophysical properties, the mean velocity and Reynolds stress fields were solved first by numerical solution of the boundary layer forms of the conservation equations for mass and momentum in conjunction with reduced forms of the transport equations for k and applicable to fully developed rectangular duct flow (cf. Demuren and Rodi [16]). An algebraic Reynolds stress model was developed to effect closure by considering the exact form of the Reynolds stress transport equations, namely:

$$\begin{aligned} \frac{D\overline{u_i u_j}}{Dt} = & - \left(\overline{u_i u_k} \frac{\partial U_j}{\partial X_k} + \overline{u_j u_k} \frac{\partial U_i}{\partial X_k} \right) + \frac{p}{\rho} \left(\frac{\partial u_i}{\partial X_j} + \frac{\partial u_j}{\partial X_i} \right) \\ & - \frac{\partial}{\partial X_k} \left\{ \overline{u_i u_j u_k} - \nu \frac{\partial \overline{u_i u_j}}{\partial X_k} + \frac{p}{\rho} (\delta_{jk} u_i + \delta_{ik} u_j) \right\} \\ & - 2\nu \frac{\partial u_i}{\partial X_k} \frac{\partial u_j}{\partial X_k} \end{aligned} \quad (1)$$

The convection and diffusion terms in the above equation were modeled using Rodi's approximation, i.e.,

$$\frac{D\overline{u_i u_j}}{Dt} - Diff_{ij} = \frac{\overline{u_i u_j}}{2k} (P_k - \epsilon) \quad (2)$$

where $Diff_{ij}$ corresponds to the third term on the RHS of Eq. (1). The second (pressure-strain) term on the RHS was modeled as a linear combination of the groups shown in Table 1 which correspond to Rotta's linear return to isotropy model ($\pi_{ij,1} + \pi_{ji,1}$) and the models

Table 1 Modelling of the pressure-strain correlation term

$\pi_{ij,1} + \pi_{ji,1}$	$-C_1 \frac{\epsilon}{k} (\overline{u_i u_j} - \frac{2}{3} k \delta_{ij})$
$\pi_{ij,2} + \pi_{ji,2}$	$-\frac{C_2 + 8}{11} (P_{ij} - \frac{2}{3} P_k \delta_{ij}) + \zeta k (\frac{\partial U_i}{\partial x_j} + \frac{\partial U_j}{\partial x_i}) - \frac{8C_2 - 2}{11} (D_{ij} - \frac{2}{3} P_k \delta_{ij})$
$[\pi_{ij} + \pi_{ji}]_w$	$C_1 = C_1^* + C_1' f(\frac{L}{X_w}) \quad C_2 = C_2^* + C_2' f(\frac{L}{X_w})$ $\zeta = \zeta^* + \zeta' f(\frac{L}{X_w})$
$P_{ij} = -\overline{u_i u_k} \frac{\partial U_j}{\partial x_k} - \overline{u_j u_k} \frac{\partial U_i}{\partial x_k}$	$D_{ij} = -\overline{u_i u_k} \frac{\partial U_k}{\partial x_j} - \overline{u_j u_k} \frac{\partial U_k}{\partial x_i}$
$P_k = -\overline{u_k u_l} \frac{\partial U_k}{\partial x_l}$	$f(\frac{L}{X_w}) = \frac{C_\mu^{\frac{3}{4}} k^{\frac{3}{4}}}{\kappa \epsilon X_w}$

Table 2 Model constant of the pressure-strain correlation term

C_1^*	C_2^*	ζ^*	C_1'	C_2'	ζ'	C_μ	κ
1.4	0.44	-0.16	-0.35	0.12	-0.1	0.09	0.42

proposed by Sugiyama et al. [17] for simulating mean strain rate ($\epsilon_{ij,2^+}$ $\epsilon_{ij,2}$) and wall proximity (ϵ_{ij,w^+} $\epsilon_{ij,w}$) effects. The coefficient values specified in Table 2 are the same as those prescribed by Sugiyama et al. [11] in previous related calculations. Inasmuch as wall functions were used in the present study for the computations, the dissipation rate everywhere in the computed flow was assumed to be locally isotropic; i.e.

$$\epsilon_{ij} = 2\nu \frac{\partial u_i}{\partial X_k} \frac{\partial u_j}{\partial X_k} = \frac{2}{3} \delta_{ij} \epsilon \quad (3)$$

The above-specified turbulence model has been successfully applied by Sugiyama et al. [11] to predict the mean flow and Reynolds stress fields in a square duct with one roughened wall for the same operating conditions as those considered in the present study. Accordingly, these results were used as input velocity for the present calculations, which focus on the mean temperature and three kinds of turbulent heat flux fields, as calculated by means of three different turbulent heat flux models.

Temperature field model

The mean temperature and turbulent heat flux fields were calculated from the boundary layer form of the thermal energy equation in conjunction with three algebraic models for the turbulent heat flux correlation which appears in this equation. The development of these models starts with the exact form of the turbulent heat flux transport equation, namely:

$$\begin{aligned} \frac{Du_i T'}{Dt} = & - \left(\overline{u_i u_j} \frac{\partial T}{\partial X_j} + \overline{u_j T'} \frac{\partial U_i}{\partial X_j} \right) + \frac{p}{\rho} \left(\frac{\partial T'}{\partial X_i} \right) \\ & - \frac{\partial}{\partial X_j} \left(\overline{u_i u_j T'} + \frac{p}{\rho} T' \delta_{ij} \right) - (\nu + a) \frac{\partial T'}{\partial X_j} \frac{\partial u_i}{\partial X_j} \end{aligned} \quad (4)$$

where the terms on the RHS represent, respectively, the production of turbulent heat flux from the mean flow, the pressure-temperature gradient effect which leads to inhomogeneity among the individual heat flux components, the diffusion of turbulent heat flux, and its dissipation. The convection and diffusion terms were modeled in a manner similar to Rodi's approximation for similar terms that appear in the Reynolds stress transport equation, namely:

$$\frac{Du_i T'}{Dt} - Diff_{iT} = \frac{u_i T'}{2k} (P_k - \epsilon) \quad (5)$$

where $Diff_{iT}$ corresponds to the third term on the RHS of Eq. (4). The fourth (dissipation) term on the RHS of Eq. (4) was neglected on the basis of assumed high Reynolds number flow in this calculation. The remaining (pressure-temperature gradient) term in Eq. (5) was modeled in three different ways, as described in the following sections.

Lumley-Launder model

For the flow situation under consideration, the pressure-temperature gradient term can be expressed (exactly) as

$$\frac{p}{\rho} \frac{\partial T'}{\partial X_i} = \frac{1}{4\pi} \int \left\{ \left(\frac{\partial^2 u_i u_m}{\partial X_i \partial X_m} \right) \frac{\partial T'}{\partial X_i} + 2 \left(\frac{\partial U_i}{\partial X_m} \right) \left(\frac{\partial u_m}{\partial X_i} \right) \frac{\partial T'}{\partial X_i} \right\} \frac{dvol}{|\mathbf{X} - \mathbf{X}'|} \quad (6)$$

where the prime around quantities in parentheses on the right-hand side denotes quantities evaluated at \mathbf{X}' , which is displaced from \mathbf{X} by separation distance \mathbf{r} . The first and second parts of the integral, defined respectively as $\pi_{iT,1}$ and $\pi_{iT,2}$, represent the effects of pressure-temperature gradient interactions which lead, respectively, to slow and rapid return of the turbulent heat flux components to an isotropic state. In reference to modeling slow return effects, Lumley [18] modified the model presented by Monin [19] by introducing an anisotropic tensor into the model coefficients which yielded the following expression for $\pi_{iT,1}$:

$$\pi_{iT,1} = -c'_{iT} \frac{\epsilon}{k} \overline{u_i T'} - c'_{iT} \frac{\epsilon}{k} \left(\frac{\overline{u_i u_j}}{k} - \frac{2}{3} \delta_{ij} \right) \overline{u_j T'} \quad (7)$$

In order to model rapid return effects, the following model proposed by Lumley [18] and independently by Launder [20] was adopted:

$$\pi_{iT,2} = c_{2T} \overline{u_m T'} \frac{\partial U_i}{\partial X_m} - c'_{2T} \overline{u_m T'} \frac{\partial U_m}{\partial X_i} \quad (8)$$

Inasmuch as wall effects on the model coefficients in Eqs. (7) and (8) are important in the present study, coefficient values were evaluated from the following expressions which take into account wall proximity effects:

$$\begin{aligned} c'_{iT} = c^*_{iT} \left\{ 1 + c_{iT,w} f \left(\frac{L}{X_w} \right) \right\}, \quad c'_{iT} = c^*_{iT} \left\{ 1 + c_{iT,w} f \left(\frac{L}{X_w} \right) \right\} \\ c_{2T} = c^*_{2T} \left\{ 1 + c_{2T,w} f \left(\frac{L}{X_w} \right) \right\}, \quad c'_{2T} = c^*_{2T} \left\{ 1 + c_{2T,w} f \left(\frac{L}{X_w} \right) \right\} \end{aligned} \quad (9)$$

where the function $f(L/X_w)$ is as defined in Table 1. The coefficients with an asterisk in Eq. (9) were selected as $c^*_{iT} = 3.9$, $c^*_{iT} = -2.5$, which are close to the values specified by Launder [21] (3.8 and -2.2), and as $c^*_{2T} = 0.8$, $c^*_{2T} = 0.2$, which correspond to the values selected by Lumley [18] and Launder [20]. The wall coefficients were specified as $c_{iT,w} = 0.25$, and $c_{2T,w} = -0.46$ from comparisons with near-wall turbulence data for an assumed turbulent Prandtl number of 0.92. The composite model formed by Eqs. (7)-(9) is designated as the Lumley-Launder (LL) model in subsequent discussion.

Shin-Lumley model

Shih and Lumley [22] have adopted a more elaborate approach in which the third rank tensor, which plays an important role to form rapid term, is represented by the most general product of heat fluxes and all possible combinations of Reynolds stress anisotropies. Besides, satisfying the kinematic constraints and realizability condition could be imposed. Application of these constraints led to the remarkably simple result as following form:

$$\pi_{ir,2} = 0.8\overline{u_k T'} \frac{\partial U_i}{\partial x_k} - 0.2\overline{u_k T'} \frac{\partial U_k}{\partial x_i} + 0.15 \frac{\varepsilon}{K} \overline{u_i T'} \left(\frac{P_k K}{\varepsilon} \right) + 0.1\overline{u_k T'} a_{ij} \left[\frac{\partial U_j}{\partial x_k} - 4 \frac{\partial U_k}{\partial x_j} \right] + 0.2\overline{u_k T'} a_{ki} \frac{\partial U_i}{\partial x_j} \quad (10)$$

where

$$a_{ij} = \left(\frac{\overline{u_i u_j}}{k} - \frac{2}{3} \delta_{ij} \right) \quad (11)$$

In the above equation, a_{ij} is Reynolds stress anisotropy tensor. Values for the model coefficients of the above rapid term were maintained constant in the computations, so that wall proximity effects were not taken into account in applying this model. In reference to modeling slow return effects for SL model, Eq. (7) is adopted in this calculation.

Craft-Launder model

Craft and Launder [23] have presented the rapid term by imposing constraints on third-rank tensor which is different from the third-rank tensor proposed by SL and LL models. The third-rank tensor of SL model includes a triple product of the anisotropic Reynolds stress, however, that of CL model is composed of double products, which point is different from each other. At the same time, they have proposed the slow term including time-scale-ratio and temperature gradient. Furthermore, Craft and Launder [24] have proposed the modified slow term to predict impinging turbulent flow. They have reported that the computed distribution of Nusselt number employing the modified slow term is good agreement with the measured profile. Therefore, the modified slow term is adopted in this research in order to evaluate the capability of prediction.

The slow and rapid terms of CL model are shown following equations, respectively.

$$\pi_{ir,1} = -1.7 \left[1 + 1.2(A_2 A_3)^{1/2} \right] R^{1/2} \frac{\varepsilon}{k} \left[\overline{u_i T'} (1 + 0.6A_2) - 0.8a_{ik} \overline{u_k T'} + 1.1a_{ij} a_{jk} \overline{u_j T'} \right] - 0.2A^{1/2} R k a_{ij} \frac{\partial T}{\partial x_j} \quad (12)$$

where

$$\left. \begin{aligned} A &= 1 - \frac{9}{8}(A_2 - A_3) \\ A_2 &= a_{ij} a_{ij} \\ A_3 &= a_{ij} a_{jk} a_{ki} \end{aligned} \right\} \quad (13)$$

In the above equation, the value of time-scale ratio R is selected the constant 0.75 in the CL model and stress invariant A consists of second and third invariants, A_2 , A_3 . In this calculation, the constant 0.75 is adopted as well as the CL model.

$$\pi_{ir,2} = 0.8\overline{u_k T'} \frac{\partial U_i}{\partial x_k} - 0.2\overline{u_k T'} \frac{\partial U_k}{\partial x_i} + \frac{1}{6} \frac{\varepsilon}{k} \overline{u_i T'} (P_{ik} / \varepsilon) - 0.4\overline{u_k T'} a_{ij} \left[\frac{\partial U_j}{\partial x_k} + \frac{\partial U_i}{\partial x_j} \right] + 0.1\overline{u_k T'} a_{ik} a_{ml} \left[\frac{\partial U_m}{\partial x_j} + \frac{\partial U_l}{\partial x_m} \right] - 0.1\overline{u_k T'} (a_{mk} P_{mk} + 2a_{mk} P_{mm}) + 0.15a_{mk} \left[\frac{\partial U_k}{\partial x_j} + \frac{\partial U_j}{\partial x_k} \right] (a_{mk} \overline{u_j T'} - a_{mi} \overline{u_k T'}) - 0.05a_{ml} \left[7a_{mk} \left[\overline{u_i T'} \frac{\partial U_k}{\partial x_j} + \overline{u_k T'} \frac{\partial U_i}{\partial x_j} \right] - \overline{u_k T'} \left[a_{ml} \frac{\partial U_i}{\partial x_k} + a_{mk} \frac{\partial U_l}{\partial x_j} \right] \right] \quad (14)$$

As shown in the above equation, it may be pointed out as a characteristic feature that the rapid term of CL model is

composed many terms compared with other models, which is expected to predict the complicated heat transfer better than other models. The values for the model coefficients were maintained constant in the computations (to observe the predictive capabilities of the CL model in its original form), so that wall proximity effects were not taken into account in applying model.

Numerical method

Inasmuch as the cross section of the square duct is symmetric about the plane $X_2 = 0$ (refer to Fig.1), the calculations were performed relative to half of the duct cross section. Fully developed flow and heat transfer in a smooth walled duct with one roughened wall was assumed. The operating Reynolds number was specified as 6.5×10^4 and all duct walls were assumed to be at the same constant temperature. These conditions correspond to the experimental operating conditions of Hirota et al. [13], whose data are used for purposes of comparison in this study. Computations were performed relative to a 22×44 uniform grid in the duct half cross section, with the first grid line near each wall located in the log-law layer, as confirmed by comparison with the data of Hirota et al. [13]. In the present study, the velocity field was calculated first, and then the temperature field, using velocity field results as input for the temperature field calculations. This procedure presumes that the velocity field is unaffected by heated flow conditions, an assumption justified by the isovelocity contours presented by Hirota et al. [13] which are essentially coincident for isothermal and heated conditions. In calculation, constant wall temperature has been set as boundary condition, which is the same as the experimental condition.

The conventional wall functions for k and ω were specified along the first grid line near each wall. On the line adjacent to the roughened wall, the log-law velocity distribution measured by Fujita et al. [2] was applied, namely

$$\frac{U_1}{U_\tau} = \frac{1}{0.42} \ln \left(\frac{U_\tau y}{\nu} \right) - 8.4 \quad (15)$$

which also was applied at grid points on the corner bisector near each smooth/rough wall intersection. Along the first grid line adjacent to each smooth wall, the conventional form of the log-law was specified; i.e.,

$$\frac{U_1}{U_\tau} = \frac{1}{0.42} \ln \left(\frac{U_\tau y}{\nu} \right) + 5.5 \quad (16)$$

In the numerical calculations a staggered grid was used and the convection terms in the governing equations were discretized by means of QUICK (third-order upwind differencing). The diffusion terms in the turbulence kinetic energy and dissipation rate equations were discretized by applying PLDS (power law differencing scheme). The solution of the pressure field was obtained by making use of SIMPLE which enabled the mean pressure and velocity fields to be determined through repeat calculations until continuity was satisfied.

RESULTS AND DISCUSSION

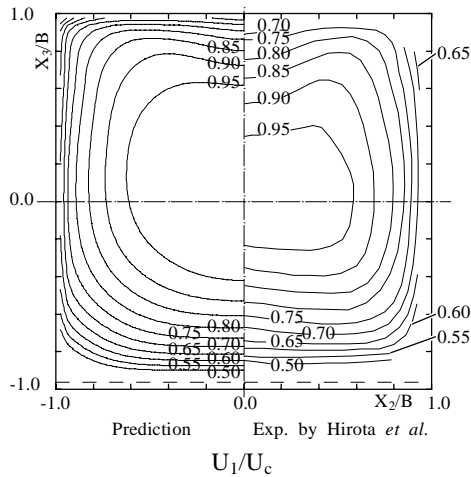


Figure 2 Comparison of mean velocity distribution

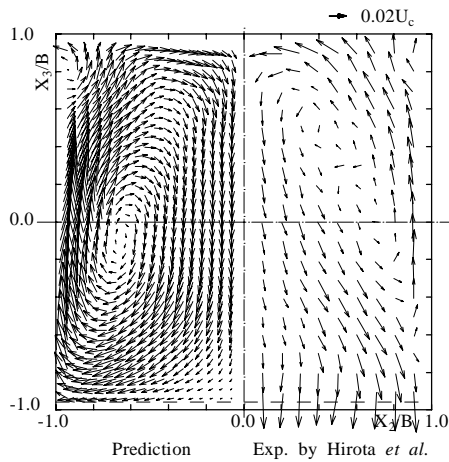


Figure 3 Comparison of secondary flow of the second kind in cross section

Mean velocity distributions

Although comparisons between predicted and measured mean velocity distributions have already been presented in an earlier paper (Sugiyama et al. [11]), primary and secondary flow velocity distributions are shown in Figs. 2 and 3, respectively, in order to demonstrate the effect of one roughened wall on the cross-sectioned mean flow pattern in a square duct for fully developed flow conditions. In Fig. 2 contour values of the primary flow velocity component U_1 are normalized by the axial centerline velocity U_c . The secondary flow velocity vectors in Fig. 3 represent the vector sum of U_2 and U_3 normalized by U_c . The dashed line above the lower wall in both figures represents the height of the ribs in the experiments of Hirota et al. [12], [15]. Fig. 2 shows that predicted primary velocity contours are in relatively good agreement with their experimental counterparts over much of the duct cross section, except in the central region where predicted contour levels slightly exceed experimental values. The secondary flow velocity vectors in Fig. 3 show that the

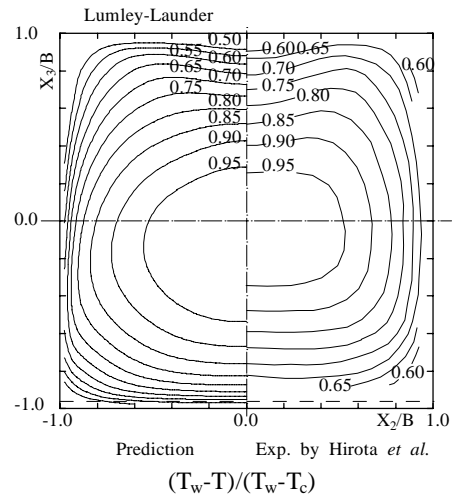


Figure 4 Temperature distribution for LL model

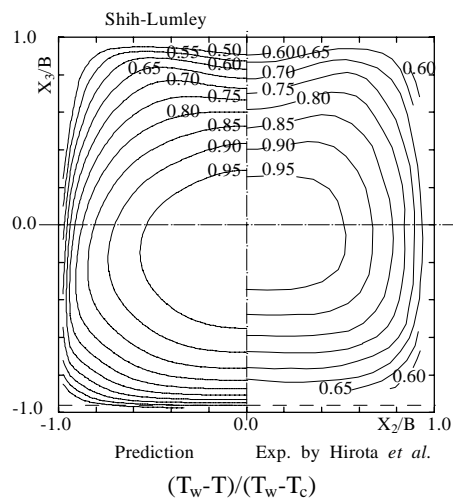


Figure 5 Temperature distribution for SL model

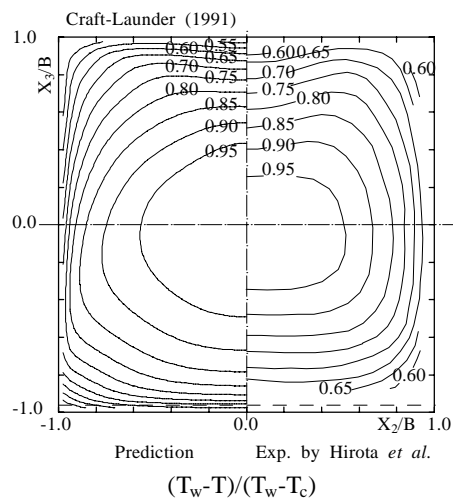


Figure 6 Temperature distribution for CL model

experimentally observed, large counter-clockwise cell is simulated well by the predictions. The computations also show, however, that a much smaller counter-rotating cell is predicted near the corner where adjacent smooth

walls intersect (at $X_2/B = -1.0$, $X_3/B = 1.0$). This cell is not readily evident in the experimental pattern. It should be noted, however, that Naimi and Gessner [9] have shown that this small cell is also predicted when alternate turbulence models are employed, namely the $k - \epsilon$ transport equation model proposed by Demuren and Rodi [16], and the Reynolds stress transport equation model developed by Naimi and Gessner [10]. It would appear, therefore, that the small cell observed in the predictions of Fig. 3 is a real effect.

Mean temperature distributions and turbulent heat flux distributions

Mean temperature contours calculated by applying the LL, SL and CL turbulent heat flux models are compared with experimental contours in Figs. 4, 5 and 6, where the temperature difference $T_w - T$ is normalized by $T_w - T_c$, with T_w and T_c defined as (uniform) wall temperature and axial centerline temperature, respectively. Following points can be pointed out as a characteristic features from the contour map of experimental mean temperature. The first point is that the distorted contour lines are recognized near the smooth wall, which is located on the opposite side of roughened wall. These distorted contour lines are caused by the secondary flow of the second kind so that it is indispensable to predict precisely its secondary flow in order to reproduce the mean temperature contours. As the second point, minimum value of temperature is generated in the bottom side from the center of square duct. Judging from these characteristic features of experimental data, a comparison of these three figures shows that any model can predict the mean temperature favorably. Since the SL model is defined as the model that additional term including Reynolds stress anisotropy tensor is added to the rapid term of the LL model as shown in Eqs. (8) and (10), results based on the LL model are similar to that based on the SL model. From this point of view, the calculated results of the CL model is a little bit different from calculated results of other two models, because the slow term is proposed in different formulation and rapid terms are composed of more additional terms compared with the other two models.

Figs. 7, 8 and 9 compare LL, SL and CL model predictions of the turbulent heat flux component $\overline{u_1 T'}$ with experimental results obtained by Hirota et al. [13]. In general, all models tend to overpredict contour levels in the upper half of the duct ($0 < X_3/B < 1$). The LL and SL model underpredict contour levels in the lower half of the duct ($-1 < X_3/B < 0$), but the CL model predicts experimental value greater than the other model, which phenomenon is specially recognized near the roughened wall. In the immediate vicinity of lower roughened wall, contour levels predicted by the LL and SL model are in relatively good agreement with experimental levels (Figs. 7 and 8), but contour levels predicted by the CL model are excessively high (Fig. 9). In contrast, figures 7 and 8 also show that the LL and the SL model lead to predicted $\overline{u_1 T'}$ levels in the central region of the duct that are

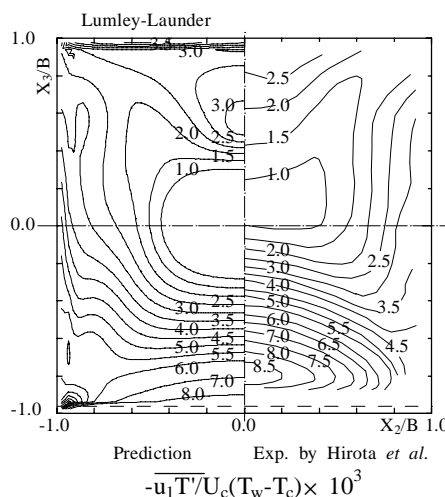


Figure 7 Primary turbulent heat flux distribution for LL model

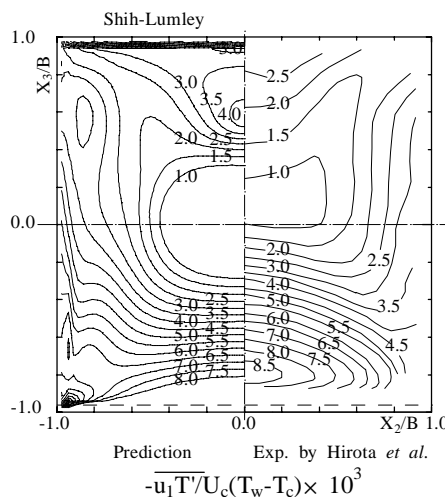


Figure 8 Primary turbulent heat flux distribution for SL model

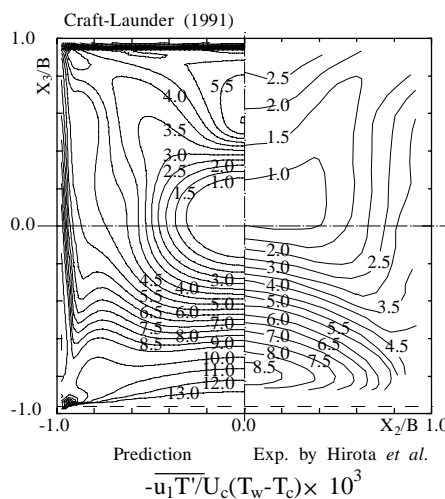


Figure 9 Primary turbulent heat flux distribution for CR model

excessively low in comparison to their experimental counterparts. On the other hand, the CL model predicts the contour line that has the value of 1.0 better than the other models. It should also be noted that none of these models is able to simulate experimentally observed contour behavior in the octant between the roughened wall and the bisector of the corner formed by this wall and the adjacent smooth wall.

Predicted contours of the turbulent heat flux component $\overline{u_2 T'}$ are compared with the experimental results of Hirota et al. [13] in Figs. 10, 11 and 12. As shown in these figures, distribution of $\overline{u_2 T'}$ is characterized by forming the positive and negative sign regions. These figures show that there is fair agreement between predicted and experimental contour levels, with three models leading to steeper gradients than those observed experimentally. All models are also unable to simulate the experimentally observed peaking characteristic of contours measured near the side wall. The experimental results near the smooth wall opposite the roughened wall appear to indicate the presence of a closed contour pattern. With reference to this closed contour that has the absolute value of 0.6, it can be said that the SL model simulates a little bit better than the other models

Experimentally measured $\overline{u_3 T'}$ contours are compared with predictions by the LL, SL and CL models in Figs. 13, 14 and 15, respectively. The experimental contours show that $\overline{u_3 T'}$ changes sign in the X_3 (vertical) direction, with the zero line nominally aligned with horizontal bisector of the duct cross section ($X_3 = 0$). Although three kinds of models are able to reproduce this behavior well, it is the CL model to predict well the zero line location as being midway between the horizontal bisector and the roughened wall that is close to the experimental result. It has been pointed out as a discrepancy between calculated result and experimental result that all models tends to overpredict $\overline{u_3 T'}$ values in the upper half of the duct, and negative contour levels predicted by all models near the roughened wall are larger in magnitude than experimentally observed values. Reviewing the comparison results of turbulent heat fluxes with experiment, it has been found that all models are unable to reproduce satisfactory the distribution of turbulent flux $\overline{u_3 T'}$.

As introduced features for three kinds of models in the above chapter, the CL model is expected to predict precisely the complicated heat transfer phenomenon because of considering more additional terms into slow and rapid terms. However, it can't be said that the CL model is especially excellent compared with the other two models, judging from the comparison results for mean temperature and turbulent heat flux distributions. In other words, these calculated results suggest that the turbulent heat transfer in a square duct with one roughened wall can be predicted sufficiently by even the LL and SL models represented as basic and simple

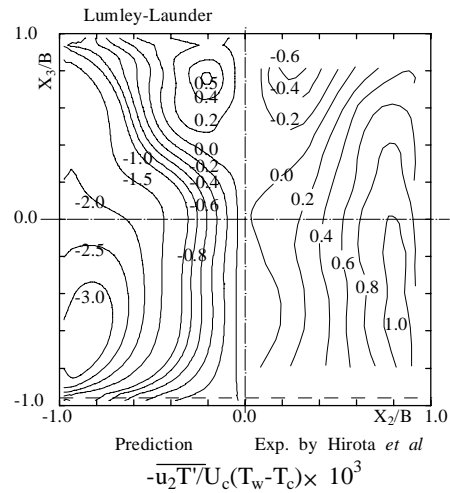


Figure 10 Horizontal turbulent heat flux distribution for LL model

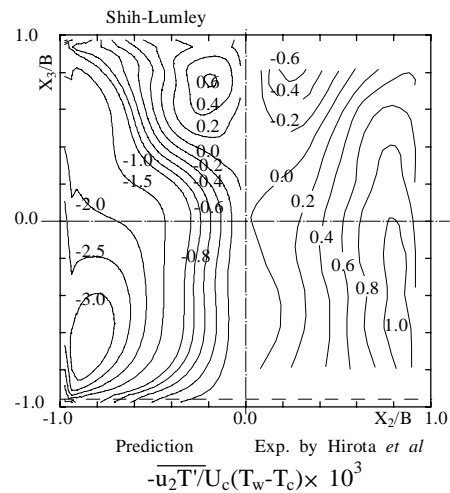


Figure 11 Horizontal turbulent heat flux distribution for SL model

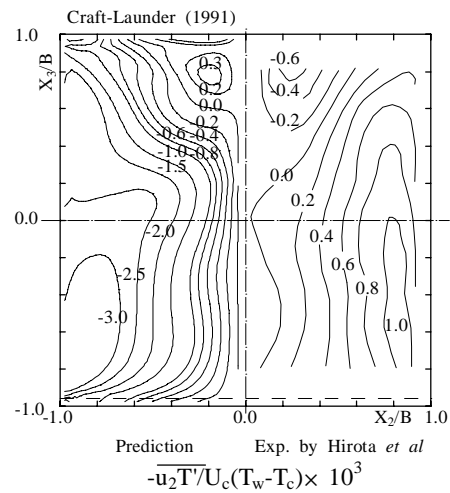


Figure 12 Horizontal turbulent heat flux distribution for CL model

model.

CONCLUSIONS

The predictive capabilities of three algebraic turbulent heat flux models have been analyzed by means of comparisons with data obtained for fully-developed flow and heat transfer in a square duct having one roughened wall and with all four walls maintained at a constant elevated temperature. Three models for the pressure-temperature gradient term in the turbulent heat flux transport equation were considered, namely the Lumley and Launder (LL) model, as defined in this study, Shin and Lumley (SL) model, and Craft and Launder (CL) model that is originally formulated by the authors. One of main difference between these models is that the rapid term of CL model is composed of many terms compared with the LL model and SL model so that it is expected to predict satisfactory the complicated turbulent heat transfer. On the basis of the comparisons made in this study, it was found that all model performed without great discrepancy with the experiment, not only with respect to predicting turbulent heat flux component behavior, but also with respect to predicting the mean temperature field. At the same time, these calculated results suggest that this turbulent heat transfer with roughened wall can be predicted by using basic and simple models such as the LL model and the SL model. Discrepancies still exist, however, between predictions and experiment which demonstrate the need for further work in this area. These include the inability of either model to predict the experimentally observed peaking characteristic of $\overline{u_1 T'}$ near the roughened wall and of $\overline{u_2 T'}$ near the adjacent side wall. Any models also predict gradients of $\overline{u_2 T'}$ in the duct cross section which are much steeper than their experimental counterparts. Contour levels of $\overline{u_3 T'}$ predicted by all models are in fair agreement with experimental values, and change sign to follow the data, but all models tends to overpredict $\overline{u_3 T'}$ values in the upper half of the duct, and negative contour levels predicted by all models near the roughened wall are larger in magnitude than experimentally observed values.

REFERENCES

- [1] Humphrey, J.A.C., and Whitelaw, J.H., "Turbulent flow in a duct with roughness," *Turbulent Shear Flows2*, Springer-Verlag, Berlin Heidelberg, Germany, (1980), pp.174-188.
- [2] Fujita, H., Yokosawa, H., Hirota, M., and Nagata, C., "Fully developed flow and heat transfer in a square duct with two roughened facing walls," *Chem. Eng. Comm.* 74, (1988), pp.95-110.
- [3] Fujita, H., Yokosawa, H., and Hirota, M., "Secondary flow of the second kind in rectangular ducts with one rough wall," *Exp. Therm. Fluid Sci.* 2(1), (1989), pp.72-80.
- [4] Fujita, H., Hirota, M., and Yokosawa, H., "Experi-

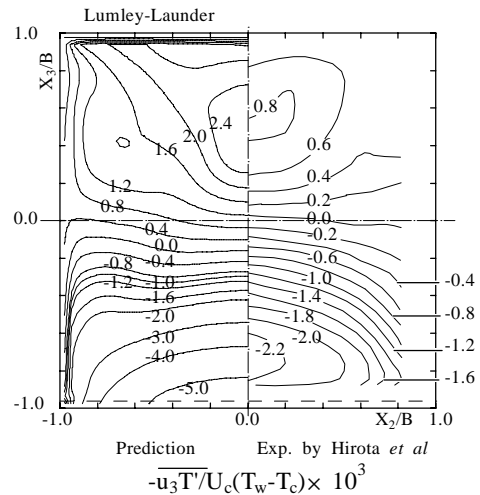


Figure 13 Vertical turbulent heat flux distribution for LL model

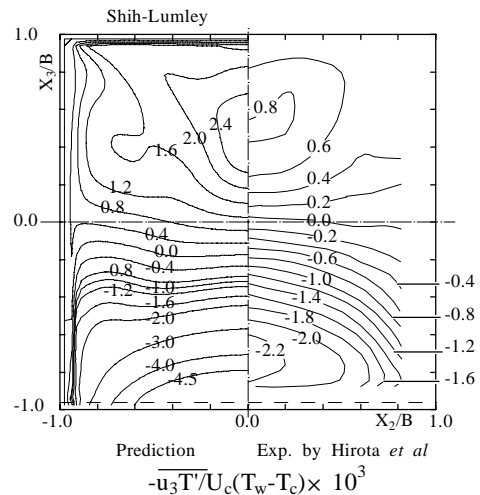


Figure 14 Vertical turbulent heat flux Distribution for SL model

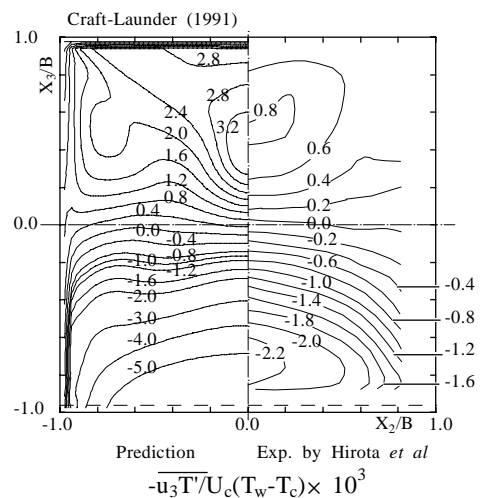


Figure 15 Vertical turbulent heat flux Distribution for CL model

- ments on turbulent flow in a square duct with a rough wall," *Memoirs of the Faculty of Engineering, Nagoya University* 41 (2), (1990), pp. 280-294.
- [5] Yokosawa, H., Fujita, H., Hirota, M., and Iwata, S., "Measurement of turbulent flow in a square duct with roughened walls on two opposite sides," *Int. J. Heat and Fluid Flow* 10 (2), (1989), pp.125-130.
- [6] Sugiyama, H., Akiyama, M., Matsumoto, M., and Hirata, M., "Numerical analysis of fully developed turbulent flow in a square duct with a rough wall," *Trans. JSME*,(in Japanese),Vol59, No.561, B(1993), pp. 1510-1517
- [7] Gessner, F. B., and Eppich, H.M., "A near-wall pressure strain model for turbulent corner flows," *Proc. 3rd Symp. Turb. Shear Flows, University of California- Davis*, (1981), pp. 2.25-2.32.
- [8] Rodi, W., "A new algebraic relation for calculating the Reynolds stresses," *ZAMM* (56), (1976), pp. T219-T221.
- [9] Naimi, M., and Gessner, F.B., "Calculation of fully-developed turbulent flow in rectangular ducts with non-uniform wall roughness," *J. Fluids Eng., Trans. ASME* 119 (3), (1997), pp.550-558.
- [10] Naimi, M., and Gessner, F. B., A calculation method for developing turbulent flow in rectangular ducts of arbitrary aspect ratio. *J. Fluids Eng., Trans. ASME* 117 (6), (1995), pp.249-258.
- [11] Sugiyama, H., Akiyama, M., and Matsumoto, M., "Numerical analysis of turbulent structure and heat transfer in a square duct," *Proc. ASME/JSME Thermal Engineering, Book No. H0933A, ASME, New York*, (1995), pp.409-416.
- [12] Hirota, M., Fujita, H., and Yokosawa, H., "Experimental study on convective heat transfer for turbulent flow in a square duct with a ribbed rough wall (Characteristics of mean temperature field)," *J. Heat Trans., Trans. ASME* 116 (5), (1994), pp.332-340.
- [13] Hirota, M., Koarai, G., Fujita, H., Nakamura, S., and Itakura, S., "Turbulent heat transfer in a square duct with a rough wall," *Trans. JSME*,(in Japanese),Vol. 67, No.653, B(2001), pp. 154-161.
- [14] Sugiyama, H., Akiyama, M., Nemoto, Y., and Gessner, F. B., "Calculation of turbulent heat flux distributions in a square duct with one roughened wall by means of algebraic heat flux models," *Int. J. Heat and Fluid Flow* 23, (2002), pp.13-21.
- [15] Hirota, M., Fujita, H., Itakura, S., and Yuasa, H., "Turbulent heat transfer in square ducts with rough walls," *Proc. 34th National Heat Transfer Conference, (in Japanese)*, (1997), pp.347-348.
- [16] Demuren, A. O., and Rodi, W., "Calculation of turbulence-driven secondary motion in non-circular ducts," *J. Fluid Mech.* 140, (1984), pp.189-222.
- [17] Sugiyama, H., Akiyama, M., and Serizawa, T., "Numerical analysis of developing flow in a square duct using Reynolds stress model," *Proc. ASME/JSME Thermal Engineering, 3, ASME, New York*, (1991), pp.159-165.
- [18] Lumley, J. L., "Introduction. In Prediction methods for turbulent flows," *Lecture Series 76, von Karman Inst., Belgium*, 1975.
- [19] Monin, A. S., "On the symmetry properties of turbulence in the surface layer of air," *Atmos. and Oceanic Phys.* 1 (1), (1965), pp.25-30.
- [20] Launder, B. E., "Progress in the modelling of turbulent transport. In Prediction methods for turbulent flow," *Lecture Series 76, von Karman Inst., Belgium*, 1975.
- [21] Launder, B. E., "Heat and mass transport," In *Turbulence, Topics in Applied Physics 12, Springer-Verlag, Berlin Heidelberg, Germany*, 1976, pp.231-287.
- [22] Shih, T-H., and Lumly, J.L., "Modeling of pressure correlation terms in Reynolds stress and scalar flux equations," *Report FDA-85-3, (1985), Sibley School of Mech. and Aerospace Eng., Cornell University*,
- [23] Craft, T. J., and Launder, B.E., "A new model for the pressure/scalar-gradient correlation and its application to homogeneous and inhomogeneous free shear flows," 7th sym. on Turbulent Shear Flows, (1989), pp.17.1.1-17.1.6.
- [24] Craft, T. J., Launder, B.E., "Computation of impinging flows using second-moment closures," 8th sym. on Turbulent Shear Flows, (1991), pp.8-5-1- 8-5-6.